

Single-hole one-electron superexcited states and doubly-excited states of molecules as studied by coincident electron-energy-loss spectroscopy

Takeshi Odagiri,
Hironobu Fukuzawa,
Ken Takahashi,
Noriyuki Kouchi,
Yoshihiko Hatano

Abstract The single-hole one-electron superexcited states and doubly-excited states of H_2 , D_2 , N_2 and O_2 have been investigated by means of the coincident electron-energy-loss spectroscopy that we developed. In this method the electron-energy-loss spectra tagged with the vacuum ultraviolet fluorescences emitted by the neutral fragments produced from superexcited molecules are measured by means of electron–photon coincidence technique. The contribution from ionization in this sort of electron-energy-loss spectra is suppressed to a large extent, and thus the structures attributed to the superexcited states of molecules become highlighted. The comparison with the photoexcitation experiments by means of the oscillator strengths give us clear discrimination between allowed and forbidden superexcited-states. As to H_2 , D_2 , and N_2 , the doubly-excited states including those found in the present experiment have been investigated in terms of both their energies and dynamical behavior. A new possibility of the coincident electron-energy-loss spectroscopy has been established in investigating the single-hole one-electron superexcited states of O_2 : the time-resolved coincident electron-energy-loss spectrum has been measured to distinguish between the direct process producing excited oxygen atoms and indirect one due to cascade transition. It has turned out that the coincident electron-energy-loss spectroscopy is a key tool for investigating superexcited molecules.

Key words doubly-excited molecule • electron-energy-loss spectroscopy • H_2 • N_2 • O_2 • superexcited molecule

Introduction

The dynamics and spectroscopy of superexcited states of molecules, i.e. excited states embedded in ionization continuum, are subjects of current interest in atomic and molecular physics [7, 8, 13]. They decay through autoionization and neutral dissociation, which compete with each other, and unlikely to emit fluorescences since the autoionization and neutral dissociation are much faster than the radiative processes [7]. In this paper we deal with single-hole one-electron superexcited states and doubly-excited states of molecules, of which electronic energies are embedded in ionization continuum at least in a certain finite range of nuclear positions, and hence they are superexcited states of the first kind [17].

As well known the electron-energy-loss spectroscopy is a useful means to investigate excited states of atoms and molecules. However, it is difficult to apply this method to investigating superexcited states of molecules, since electron-energy-loss spectra are in general dominated by direct ionization in the range of the superexcited states. The best way to observe molecular superexcited states is thus to eliminate the contribution from ionization. We developed a new method a few years ago along the lines mentioned above, i.e. the coincident electron-energy-loss spectroscopy [20, 21]. In this method electron-energy-loss spectra tagged with the vacuum ultraviolet (VUV) fluorescence emitted by neutral fragments produced from superexcited molecules are measured by means of electron–photon coincidence technique. The contribution from ionization in this sort of spectra is suppressed to a large extent, and thus the

T. Odagiri, H. Fukuzawa, K. Takahashi,
N. Kouchi[✉], Y. Hatano^{*}
Department of Chemistry,
Tokyo Institute of Technology,
O-okayama 2-12-1, Meguro-ku, Tokyo 152-8551, Japan,
Tel.: -81-(0)3-5734-2611, Fax: -81-(0)3-5734-2655,
e-mail: nkouchi@chem.titech.ac.jp

^{*}Present address:
Department of Molecular and Material Sciences,
Kyushu University,
6-1 Kasugakoen, Kasuga, Fukuoka 816-8580, Japan

Received: 14 November 2002

structures attributed to superexcited states of molecules become highlighted.

In this paper we present the interesting results for the doubly-excited states of H_2 [21], D_2 [27], and N_2 [19] together with those for the single-hole one-electron superexcited states of O_2 obtained by means of the coincident electron-energy-loss spectroscopy.

Experiment

The experimental apparatus is composed of an electron spectrometer, a VUV photon detector, and a standard delayed-coincidence system. A VUV photon passes through an optical window and is detected by a microchannel plate: a microchannel plate without CsI coating combined with an MgF_2 window was used in the experiment for H_2 and D_2 and a microchannel plate coated with CsI combined with a LiF window was used in the experiment for N_2 and O_2 . An angle- and energy-resolved electron is detected in coincidence with a VUV photon, i.e. a coincidence time spectrum is obtained. Coincidence rates are normalized for the incident beam current, target number density and geometric factor [21, 27], and then the

normalized rates are plotted against the energy loss to obtain an electron-energy-loss spectrum tagged with the VUV fluorescence detected, i.e. a coincident electron-energy-loss spectrum. In O_2 experiment coincidence time spectra are normalized to obtain a time-resolved coincident electron-energy-loss spectrum as described in the section of O_2 . Only the Lyman- α fluorescence contributes to the coincident electron-energy-loss spectra in the experiments on H_2 and D_2 while several fluorescences from excited fragment atoms contribute to those in the experiments on N_2 and O_2 .

Results and discussion

H_2 [21] and D_2 [27]

The electron-energy-loss spectrum of H_2 tagged with the Lyman- α fluorescence, i.e. the coincident electron-energy-loss spectrum, is presented in Fig. 1b together with the ordinary electron-energy-loss spectrum in Fig. 1a, both of which were measured at 80 eV incident electron energy and 3° scattering angle, often written as 80 eV/ 3° in this paper. Two broad peaks centered at 26 and 34 eV due to doubly-excited states of H_2 are clearly seen in the coincident electron-energy-loss spectrum while no spectral features of the doubly-excited states are observed in the ordinary electron-energy-loss spectrum.

The coincident energy-loss spectrum in Fig. 1b is converted to the effective generalized oscillator strength (effective-GOS) for the formation of $H(2p)$, which is compared with the dipole oscillator strength (DOS) for the same process measured in the photoexcitation experiments [1, 4, 5]. It turns out from the comparison that the 34 eV peak is attributed to allowed doubly-excited states and the 26 eV peak is to a forbidden doubly-excited state.

A simple calculation based on the reflection approximation for the double excitation and the survival probability for the subsequent autoionization reproduces well the 34 eV peak as shown in Fig. 1b taking the three allowed doubly-excited states of H_2 , the $Q_1^1\Sigma_u^+(1)$, $Q_1^1\Pi_u(1)$, and $Q_2^1\Pi_u(1)$ states, into account in accordance with our early work [1]. The forbidden doubly-excited state for the 26 eV peak seems to have a bound potential energy curve correlating to $H(2p) + H(n=2)$ since the intensity in Fig. 1b vanishes suddenly around the dissociation limit of $H(2p) + H(n=2)$. Such a kind of doubly-excited states had not been reported. We hence obtained a potential energy curve in a way that the simple calculation reproduces the 26 eV peak. The obtained curve is shown in Fig. 2 (curve 'F'), which largely differs from the potential energy curves of other doubly-excited states of H_2 , and the curve 'F' has not been calculated theoretically [16].

There may be a possibility that the 26 eV peak is attributed to the $Q_1^1\Sigma_g^+(1)$ state, which is forbidden and the lowest doubly-excited state, since its potential energy curve crosses the right edge of the Franck-Condon region around 25 eV (see Fig. 2). However, the theoretical curve due to the $Q_1^1\Sigma_g^+(1)$ state does not fit to the 26 eV peak as shown in Fig. 1c. It seems unlikely that the $Q_1^1\Sigma_g^+(1)$ state, which is a forbidden and also highly autoionizing doubly-excited state, makes as large contribution as the allowed and less autoionizing doubly-excited states mentioned

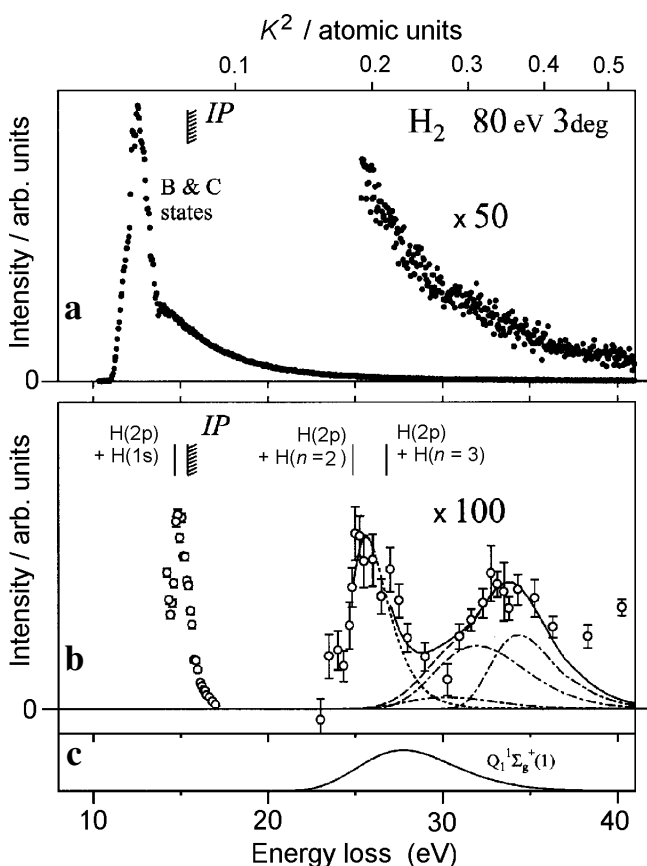


Fig. 1. The ordinary (a) and coincident (b) electron-energy-loss spectra of H_2 measured at 80 eV incident electron energy and 3° scattering angle. The first adiabatic ionization potential (IP) is shown and the dissociation limits are indicated by vertical bars. Curves in (b) represent the results of the theoretical fits (see the section of H_2 and D_2). The curve in (c) shows the theoretical curve due to the $Q_1^1\Sigma_g^+(1)$ state (see the section of H_2 and D_2). The square of the momentum transfer, K^2 , is indicated at the top of the figure. The resolution of the energy loss is approximately 250 meV.

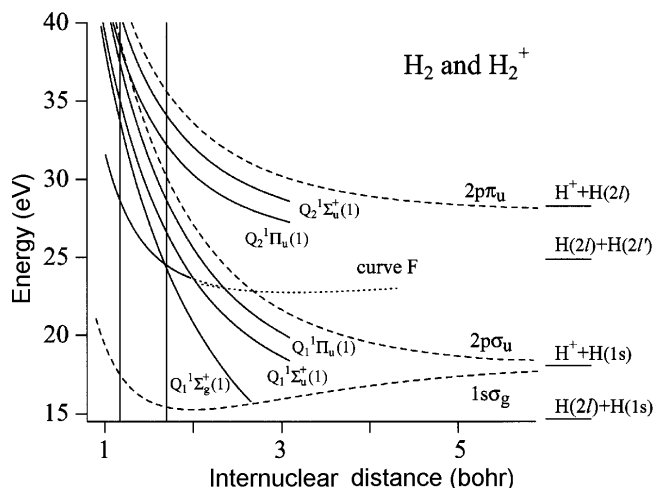


Fig. 2. Potential energy curves of the doubly-excited states of H_2 (solid curves: [6, 24]) and the three lowest states of H_2^+ (dashed curves: [23]). Curve 'F' represents the potential energy curve of the precursor doubly-excited state of the 26 eV peak (see the section of H_2 and D_2). Zero energy is taken at the lowest vibrational-rotational level of the ground electronic state of H_2 . The potential energy curves for H_2 and D_2 are the same. The Franck-Condon region for H_2 is indicated by vertical bars.

above, i.e. the $Q_1^1\Sigma_u^+(1)$, $Q_1^1\Pi_u(1)$, and $Q_2^1\Pi_u(1)$ states, in the energy-loss spectrum measured at $80\text{ eV}/3^\circ$ tagged with the neutral dissociation to form $H(2p)$. In Fig. 3 the resonance widths of those doubly-excited states are shown against the internuclear distance to display their character of autoionization: Γ/\hbar is the rate of autoionization, where Γ is the resonance width.

The integration of each fitted curve in Fig. 1b gives the relative cross section of $2p$ atom formation via each precursor doubly-excited states measured at $80\text{ eV}/3^\circ$, differential against the solid angle for scattered electrons and the solid angle for Lyman- α photons. The results in H_2 are shown in Table 1 together with those in D_2 , where the cross sections are those relative to the cross section of the forbidden doubly-excited state for the 26 eV peak in H_2 . The $Q_1^1\Sigma_u^+(1)$ state gives the smallest cross section among the three allowed doubly-excited states for the

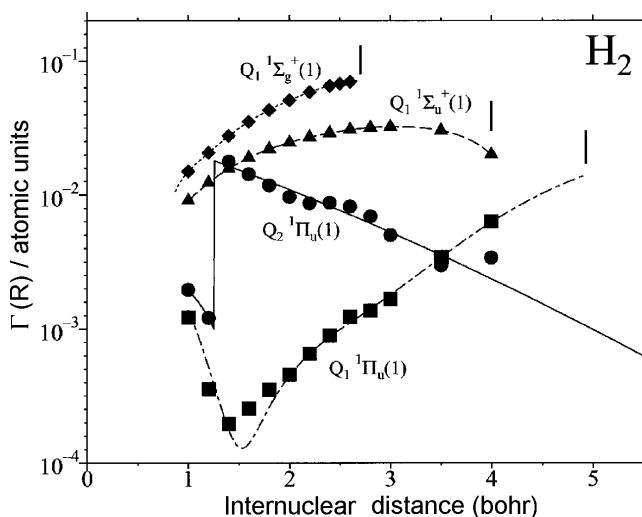


Fig. 3. Resonance widths of the $Q_1^1\Sigma_g^+(1)$, $Q_1^1\Sigma_u^+(1)$, $Q_1^1\Pi_u(1)$, and $Q_2^1\Pi_u(1)$ doubly-excited states of H_2 as a function of internuclear distance. That of the $Q_1^1\Sigma_g^+(1)$ state is from [24] and those of other states are from [26]. The curves show the results of the fitting and extrapolation by the authors to calculate the survival probability (see the section of H_2 and D_2). The short bar attached to each curve indicates the stabilization point of each doubly-excited state, where the resonance width vanishes. The resonance widths are the same for H_2 and D_2 .

34 eV peak, which seems to be attributed mainly to the widest resonance width of the $Q_1^1\Sigma_u^+(1)$ state. The $Q_1^1\Sigma_g^+(1)$ state would probably give negligible cross section since its resonance width is wider than that of the $Q_1^1\Sigma_u^+(1)$ state and the excitation cross section to the forbidden $Q_1^1\Sigma_g^+(1)$ state seems smaller than that to the allowed $Q_1^1\Sigma_u^+(1)$ state at $80\text{ eV}/3^\circ$. Again it is unlikely that the 26 eV peak originates from the $Q_1^1\Sigma_g^+(1)$ state.

In conclusion, the origin of the 26 eV peak remains controversial partly because the full quantal calculation on the dynamics of the doubly-excited molecules has not been carried out even for the simplest molecule H_2 . The efforts to reveal the origin will give us a better understanding of doubly-excited molecules.

N_2 [19]

Figure 4 shows the effective-GOSs obtained from the ordinary electron-energy-loss spectra of N_2 measured at 80 and 150 eV incident electron energies and 2° scattering angle and the DOS of N_2 [3]. The contributions of direct ionization are subtracted by using a polynomial fit, and thus they are the oscillator strengths for the double excitation. Three oscillator strengths are normalized around the energy loss of 23 eV. The similarity in shape shows that the effective-GOSs for the double excitation at $80\text{ eV}/2^\circ$ and $150\text{ eV}/2^\circ$ are dominated by the same allowed doubly-excited states as those in the DOS for the double excitation.

In Fig. 5 the effective-GOSs of N_2 for the neutral dissociation resulting in the formation of the fragments emitting VUV fluorescence, i.e. the emissive neutral-dissociation, obtained from the coincident electron-energy-loss spectra measured at $80\text{ eV}/2^\circ$ and $150\text{ eV}/2^\circ$ are shown together with the DOS of N_2 for the emissive neutral-dissociation [28]. Again three oscillator strengths

Table 1. Cross sections of $2p$ atom formation in electron impact on H_2 and D_2 via doubly-excited states at 80 eV incident electron energy and 3° scattering angle, differential against the solid angle for scattered electrons and the solid angle for Lyman- α photons^{a)}.

The forbidden state for the 26 eV peak		The allowed states for the 34 eV peak		
		$Q_1^1\Sigma_u^+(1)$	$Q_1^1\Pi_u(1)$	$Q_2^1\Pi_u(1)$
H_2	1	$\sim 0.2^{\text{d)}$	0.97	0.83
		$3.0^{\text{c)}$	$2.0^{\text{b)}$	
D_2	1.1	$\sim 0.1^{\text{d)}$	0.34	0.86
		$2.4^{\text{c)}$	$1.3^{\text{b)}$	

^{a)} The cross sections are those relative to the cross section of the forbidden doubly-excited state for the 26 eV peak in H_2 .

^{b)} The sum of the cross sections of the allowed doubly-excited states for the 34 eV peak.

^{c)} The sum of all the cross sections.

^{d)} The uncertainty is large because of the small contribution (see Fig. 1b).

are normalized around the energy loss of 23 eV. It is reasonable that the shape of the effective-GOS for the emissive neutral-dissociation at 150 eV/2° is closer to that of the DOS for the emissive neutral-dissociation than at 80 eV/2° considering the smaller values of the square of the momentum transfer, K^2 , at 150 eV/2° than at 80 eV/2° as shown on the upper axes of Fig. 5. The difference in shape between the effective-GOSs and DOS for the emissive neutral-dissociation is noticeable in contrast to Fig. 4. Figures 4 and 5 clearly indicate an important role of the forbidden doubly-excited states in the range 25–35 eV in the effective-GOSs for the emissive neutral-dissociation in Fig. 5, while they hardly contribute to the effective-GOSs for the double excitation in Fig. 4 as mentioned above. It follows that the forbidden doubly-excited states mentioned above have a much larger branching ratio into the emissive neutral-dissociation than the allowed doubly-excited states in the DOS for the emissive neutral-dissociation in Fig. 5. Existence of the allowed and forbidden doubly-excited states of N_2 and the large difference between them in their decay processes have been revealed clearly for the first time.

The large and broad hump in the range of the energy loss 25–35 eV in the effective-GOS for the emissive neutral-dissociation at 80 eV/2° in Fig. 5 seems to consist of several peaks, among which a sharp peak around 29 eV energy loss is noticeable. These peaks are not so separated in the effective-GOS at 150 eV/2°. It is unambiguous that the sharp peak around 29 eV does not appear in the DOS for the emissive neutral-dissociation in Fig. 5, indicating that the sharp peak may be attributed to a forbidden doubly-

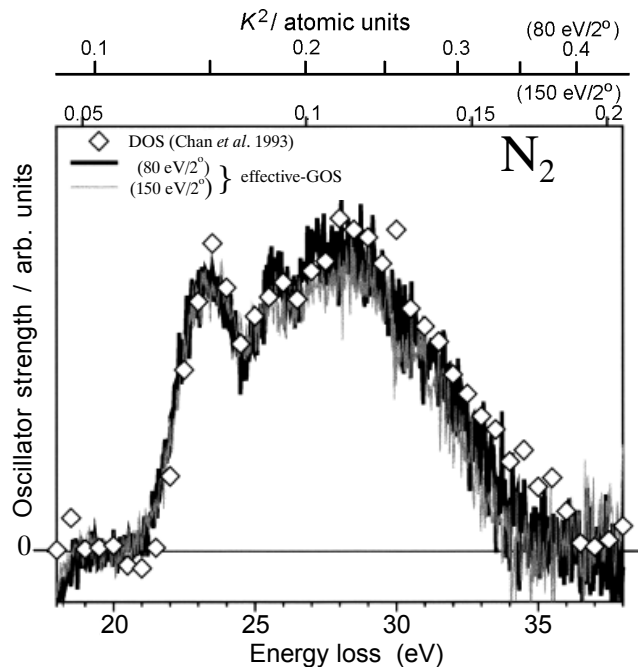


Fig. 4. The effective-GOSs of N_2 obtained from the ordinary electron-energy-loss spectra measured at 80 eV/2° (thick curve) and 150 eV/2° (thin curve) and the DOS of N_2 (open diamonds: Chan *et al.* [3]). The contributions of direct ionization are subtracted to show the oscillator strengths for the double excitation. Three oscillator strengths are normalized around 23 eV energy loss. The resolution of the energy loss in the effective-GOSs is approximately 250 meV while that in the DOS is 1 eV. The square of the momentum transfers, K^2 , in 80 eV/2° and 150 eV/2° is indicated on the upper axes.

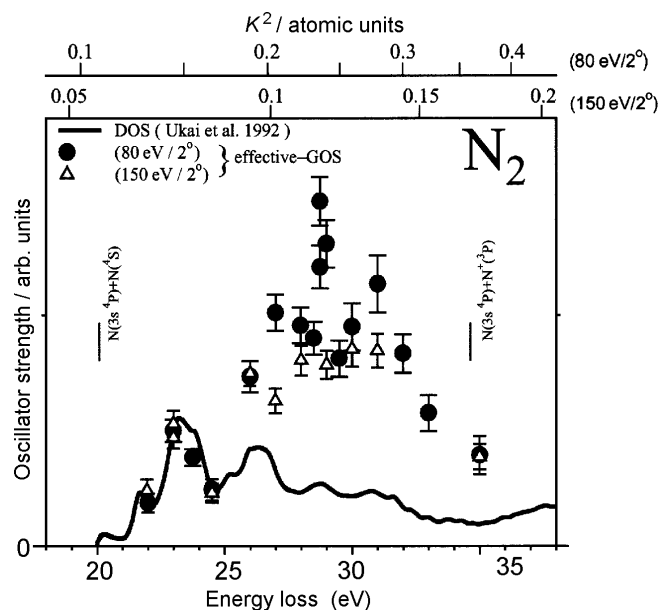


Fig. 5. The effective-GOSs of N_2 for the emissive neutral-dissociation at 80 eV/2° (closed circles) and 150 eV/2° (open triangles) obtained from the coincident electron-energy-loss spectra and the DOS of N_2 for the emissive neutral-dissociation (solid curve: Ukai *et al.* [28]). Three oscillator strengths are normalized around 23 eV energy loss. The resolution of the energy loss is approximately 250 meV. The square of the momentum transfers, K^2 , in 80 eV/2° and 150 eV/2° is shown on the upper axes. The lowest dissociation limits of the emissive neutral-dissociation and emissive dissociative-ionization are indicated by vertical bars.

excited state, probably a single vibronic level. The origin of the sharp peak is unknown at the present stage.

O_2

The ground electronic state of O_2 , $X^3\Sigma_g^-$, has the electron configuration, $(1\sigma_g)^2(1\sigma_u)^2(2\sigma_g)^2(2\sigma_u)^2(3\sigma_g)^2(1\pi_u)^4(1\pi_g)^2$ [11, 14]. We have focused on the range of the energy loss 14.5–19 eV, which corresponds to the ionization of the $1\pi_u$ and $3\sigma_g$ electrons and the major part of the photoabsorption cross sections as a function of incident photon energy with rich structures [2].

In Fig. 6 shown are the electron-VUV photon coincidence time spectra at each energy loss indicated, which were measured at 80 eV incident electron energy and 3° scattering angle. The intensity in this Figure is true coincidence rate at each channel in time normalized for the incident electron beam current, target number density and geometric factor in the following way (see also [21] and [27]).

The intensity at the j th channel is expressed by

$$(1) \quad \frac{\left(\dot{N}^t(j) / \dot{N}_{ph} \right)}{\frac{1}{2} \left\{ \left(\dot{N}^{t'} / \dot{N}_{ph}' \right) + \left(\dot{N}^{t''} / \dot{N}_{ph}'' \right) \right\}}$$

where $\dot{N}^t(j)$ is the true coincidence rate at the j th channel, \dot{N}_{ph} the count rate of the VUV photons recorded during the coincidence measurement, and $\dot{N}^t = \sum_j \dot{N}^t(j)$, i.e. the true coincidence rate; the ' and '' refer to the quantities

measured at the energy loss of 16.49 eV as reference immediately before and after the coincidence measurement at each energy-loss in Fig. 6. $\dot{N}^t(j)$ is divided by \dot{N}_{ph} to normalize for the incident electron beam current and target number density, and furthermore $\dot{N}^t(j)/\dot{N}_{ph}$ is divided by $\frac{1}{2}\{(\dot{N}^t/\dot{N}_{ph}) + (\dot{N}^t/\dot{N}_{ph})\}$ to normalize for the geometric factor, which may change slightly and slowly during the coincidence measurement. The summation of the intensities in Fig. 6, i.e. the summation of quantity (1), over the range of channel j gives

$$(2) \quad \frac{(\dot{N}^t / \dot{N}_{ph})}{\frac{1}{2}\{(\dot{N}^t / \dot{N}_{ph}) + (\dot{N}^t / \dot{N}_{ph})\}},$$

which is plotted against the energy loss to obtain the coincident electron-energy-loss spectrum at 80 eV/3°. Figure 6 turns out to show the time-resolved coincident electron-energy-loss spectrum measured at 80 eV/3°.

It is seen from Fig. 6 that:

- i) no true-coincidence peak is observed at 14.50 eV energy loss;
- ii) the sharp true-coincidence peaks that have slightly asymmetric shapes with the full widths at half maximum of approximately 3 ns are observed at 15.00, 15.50 and 16.00 eV energy loss;
- iii) the true coincidence peaks are dominated by the slow decay components at the energy loss of 16.25 eV and above;
- iv) the true coincidence peaks are much weaker at 18.50 and 18.99 eV energy loss than at the others.

The slightly asymmetric shapes mentioned in ii) indicate that they are determined almost entirely by the instrumental time resolution, several nanoseconds [21]. Table 2 lists the VUV fluorescences emitted by oxygen atoms as dissociation fragments that are detectable in our photon detector together with the lowest dissociation limits for the production of the relevant excited oxygen atoms. Some O^+ and O^{2+} fluorescences are also detectable, while they cannot contribute to the time-resolved coincident electron-energy-loss spectrum in Fig. 6 because of the energetical reasons. It follows that the time-resolved coincident electron-energy-loss spectrum is attributed to some of the fluorescences from excited oxygen atoms listed in Table 2.

Let us then discuss our findings i)–iv) mentioned above. The contribution from the 136 nm line seems negligible in the time-resolved coincident electron-energy-loss spectrum in Fig. 6 considering that the lifetime of $O^*(3s^3S)$ is 180 μ s [22, 29] and thus the contribution would be constant

Table 2. Vacuum ultraviolet fluorescences from excited oxygen atoms O^* detectable in our photon detector, i.e. a microchannel plate coated with CsI combined with an LiF window. The lowest dissociation limits refer to those of $O^* + O((2p)^4^3P)$. Data are taken from [9, 22, 25].

O^*	Transition	Wavelength (nm)	Lowest dissociation limit (eV)
$3s^5S$	$3s^5S \rightarrow (2p)^4^3P$	136	14.26
$3s^3S$	$3s^3S \rightarrow (2p)^4^3P$	130	14.64
$4s^3S$	$4s^3S \rightarrow (2p)^4^3P$	104	17.05
$3d^3D$	$3d^3D \rightarrow (2p)^4^3P$	103	17.20
$3s^1D$	$3s^1D \rightarrow (2p)^4^1D$	115	17.85
$3s^1P$	$3s^1P \rightarrow (2p)^4^1S$	122	19.49

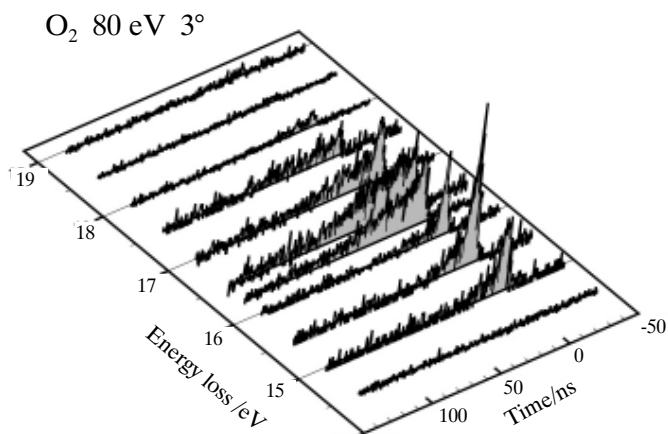
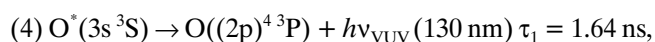
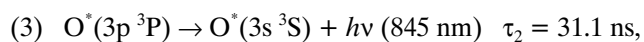


Fig. 6. The time-resolved coincident electron-energy-loss spectrum of O_2 measured at 80 eV incident electron energy and 3° scattering angle. The intensity is true coincidence rate at each channel in time normalized for the incident electron beam current, target number density and geometric factor (see (1)).

if any. The lifetime of $O^*(3s^3S)$ is 1.64 ns [22, 29] and the lowest dissociation limit for the production of $O^*(3s^3S)$, i.e. that of $O^*(3s^3S) + O((2p)^4^3P)$, is 14.64 eV (see Table 2). It hence seems that the sharp peaks at 15.00, 15.50, and 16.00 eV energy loss in Fig. 6 are attributed to the 130 nm line emitted by $O^*(3s^3S)$. This line is known to have larger cross sections than other VUV lines emitted by oxygen atoms in electron impact on O_2 [11] and plays an important role in the VUV fluorescence spectra in the photoexcitation of O_2 in the range of the incident photon energy 14.6–17.5 eV [15].

The slow decay component appears at the energy loss of 16.25 eV and above. There is a possibility that quenching of O^* atoms by O_2 molecules influences the slow decay components. In order to examine this quenching effect the time spectra were measured at 16.49 eV energy loss with varying the O_2 pressure in the gas reservoir from 1.1 to 5.4 mTorr, which is proportional to the pressure in the gas cell. The shape of the time spectra is independent of the pressure and the true coincidence rates are proportional to the pressure in the range mentioned above. It follows that the effect of the quenching of O^* atoms by O_2 molecules is negligible in the time spectra in Fig. 6 since they were measured at a pressure of approximately 2–3 mTorr in the gas reservoir.

Figure 6 shows the onset of the slow decay component lies between 16.00 and 16.25 eV energy loss, and thus there is no possibility that 104, 103 and 115 nm lines from excited oxygen atoms in Table 2 contribute to the slow decay component because the lowest dissociation limits for the production of these lines exceed the onset of the slow decay component and the lifetimes of the upper levels emitting these lines are shorter than 10 ns [22, 29]. In conclusion, the slow decay component seems to originate from a cascade transition, i.e. $O^{**} \rightarrow O^* + h\nu$, and then $O^* \rightarrow O + h\nu_{VUV}$, where $h\nu_{VUV}$ is a fluorescence photon in the VUV range. The most probable candidate is



where $h\nu$ (845 nm), for example, indicates that the wavelength of the fluorescence is 845 nm. Each radiative transition is a single decay channel of each excited oxygen atom, of which lifetime is also shown in the above [22, 29]. The dissociation limit of $O^*(3p^3P) + O((2p)^4^3P)$ is 16.10 eV [9, 22], which is between 16.00 and 16.25 eV energy loss: the slow decay component does not appear at 16.00 eV while it appears at 16.25 eV as shown in Fig. 6.

Solving the coupled rate equations for transitions (3) and (4) we obtain

$$(5) \quad n_{3s}(t) = n_{3s0} \exp(-\tau_1^{-1}t) + \frac{\tau_2^{-1}n_{3p0}}{\tau_1^{-1} - \tau_2^{-1}} \left(\exp(-\tau_2^{-1}t) - \exp(-\tau_1^{-1}t) \right),$$

where $n_{3s}(t)$ is the number density of $O^*(3s^3S)$ as a function of time t , and n_{3s0} and n_{3p0} are the number densities of $O^*(3s^3S)$ and $O^*(3p^3P)$ at $t = 0$, respectively. The origin of time t is taken as the time when $O^*(3s^3S)$ and $O^*(3p^3P)$ are produced since the excitation of O_2 and subsequent decay to produce $O^*(3s^3S)$ and $O^*(3p^3P)$ are much faster than the radiative transitions from them.

Let us try to fit $Cn_{3s}(t)$, where C is a time-independent constant, to the two time spectra with and without the slow decay component, i.e. those at 16.25 and 15.00 eV energy loss, respectively, where Cn_{3s0} and Cn_{3p0} are fitting parameters. In fact $Cn_{3s}(t)$ is folded with the time resolution of our apparatus (3 ns), and then the folded one is fitted to the measured time spectra. The result is shown in Fig. 7, where $Cn_{3s0} : Cn_{3p0} = 1:0$ at 15.00 eV energy loss and $Cn_{3s0} : Cn_{3p0} = 1:11$ at 16.25 eV energy loss. We conclude from the above discussion that the slow decay component in Fig. 6 appearing at 16.25 eV energy loss and above is attributed to the cascade transition (3) and (4), i.e. the second term of the right hand side of equation (5), while the sharp peak appearing at 15.00 eV energy loss and above is attributed to the non-cascade process, i.e. the first term of the right hand side of equation (5). The 130 nm line emitted by $O^*(3s^3S)$ plays the most important role among the VUV fluorescences in Table 2 in the time spectra of Fig. 6.

As mentioned we sum up intensity (1) over the range of j in each time spectrum of Fig. 6 to obtain the coincident electron-energy-loss spectrum at 80 eV/3°. Taking account of the above-mentioned fact that the shape of the time spectra in Fig. 6 is dependent on the energy loss, we set three ranges of j for the summation as shown in Fig. 7, i.e. the total, fast, and slow ranges, and obtain three coincident electron-energy-loss spectra accordingly as follows:

- the “total” coincident electron-energy-loss spectrum obtained from the summation over the “total” range of j , which is the same as the coincident electron-energy-loss spectra in the sections of H_2 , D_2 , and N_2 ;
- the “fast” coincident electron-energy-loss spectrum obtained from the summation over the “fast” range of j , which covers a major part of the non-cascade component, i.e. the first term of the right hand side of equation (5), and a small fraction of the slow decay component, i.e. the second term of the right hand side of equation (5);
- the “slow” coincident electron-energy-loss spectrum obtained from the summation over the “slow” range of

j , which covers a major part of the slow decay component and hardly involve the non-cascade component. The total, fast and slow coincident electron-energy-loss spectra of O_2 at 80 eV incident electron energy and 3° scattering angle are shown in Fig. 8. The slow coincident electron-energy-loss spectrum seems not to fall off to zero below 16.00 eV energy loss, which would be due to the small discrepancies between the best-fitted curves of equation (5) and the measured time spectra at 16.00, 15.50 and 15.00 eV energy loss (see the upper part of Fig. 7, for example).

The total coincident electron-energy-loss spectrum consists of two peaks around 15.5 and 16.5 eV energy loss. The peak around 15.5 eV is attributed to the non-cascade component, i.e. the production of $O^*(3s^3S)$ and its radiative decay to $O((2p)^4^3P)$ emitting the 130 nm line. The peak around 16.5 eV is attributed mainly to the slow decay component, i.e. the production of $O^*(3p^3P)$ and the subsequent cascade transition, (3) and (4), and partly to

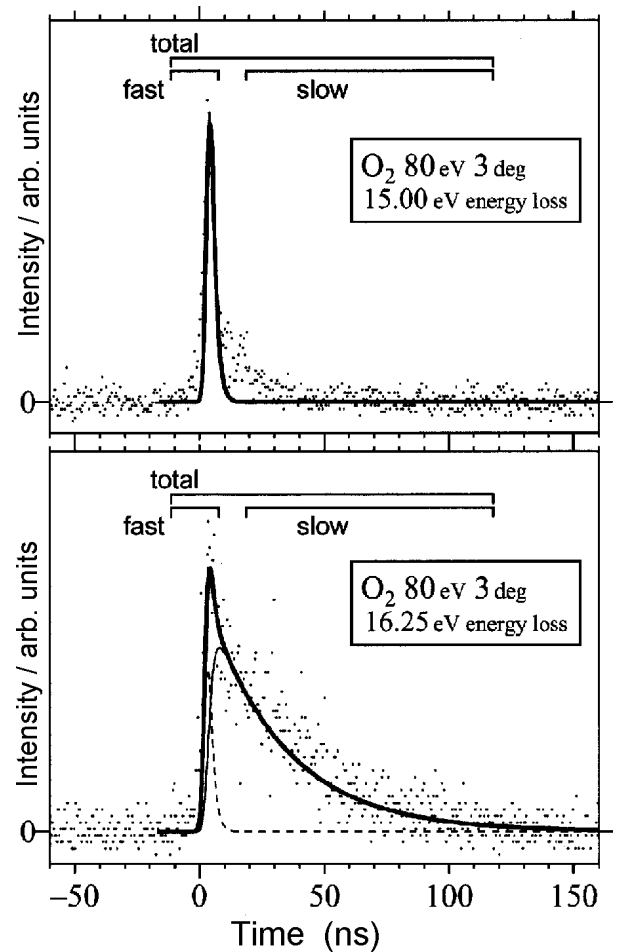


Fig. 7. Examples of the coincidence time spectra at 80 eV incident electron energy and 3° scattering angle with and without the slow decay component, i.e. those at 16.25 and 15.00 eV energy loss, respectively. The thick solid curve represents the result of the fits of $Cn_{3s}(t)$ folded with the time resolution of our apparatus (see Eq. (5) and the section of O_2). The dashed curve and thin solid curve represent the folded contributions from the first term and second term of the right hand side of equation (5), respectively. The total, fast and slow ranges are set in order to obtain the three coincident electron-energy-loss spectra as shown in Fig. 8 (see the section of O_2).

the non-cascade component mentioned just above. There is no possibility that the partner of $O^*(3s^3S)$ and $O^*(3p^3P)$ is an O^+ ion in the present range of the energy loss since the dissociation limits of $O^*(3s^3S) + O^*((2p)^34S)$ and $O^*(3p^3P) + O^*((2p)^34S)$ are 28.25 and 29.72 eV, respectively [9, 22, 25]. It follows that the peaks around 15.5 and 16.5 eV energy loss originate from the neutral dissociation from the superexcited states around 15.5 and 16.5 eV energy loss, respectively. The superexcited states around 15.5 eV produce $O^*(3s^3S)$ and those around 16.5 eV produce $O^*(3p^3P)$ and $O^*(3s^3S)$ (the former is the main product). They are single-hole one-electron superexcited states, probably built on the $a^4\Pi_u(1\pi_u)^{-1}$, $A^2\Pi_u(1\pi_u)^{-1}$, $b^4\Sigma_g^-(3\sigma_g)^{-1}$, or $B^2\Sigma_g^-(3\sigma_g)^{-1}$ state of O_2^+ , the last one of which is not involved in Fig. 8 because the adiabatic ionization potential is 20.297 eV [11].

In order to examine the contribution of forbidden superexcited states in Fig. 8, the effective-GOS for the emissive neutral-dissociation obtained from the total coincident electron-energy-loss spectrum is compared with the DOS for the emissive neutral-dissociation [15] obtained

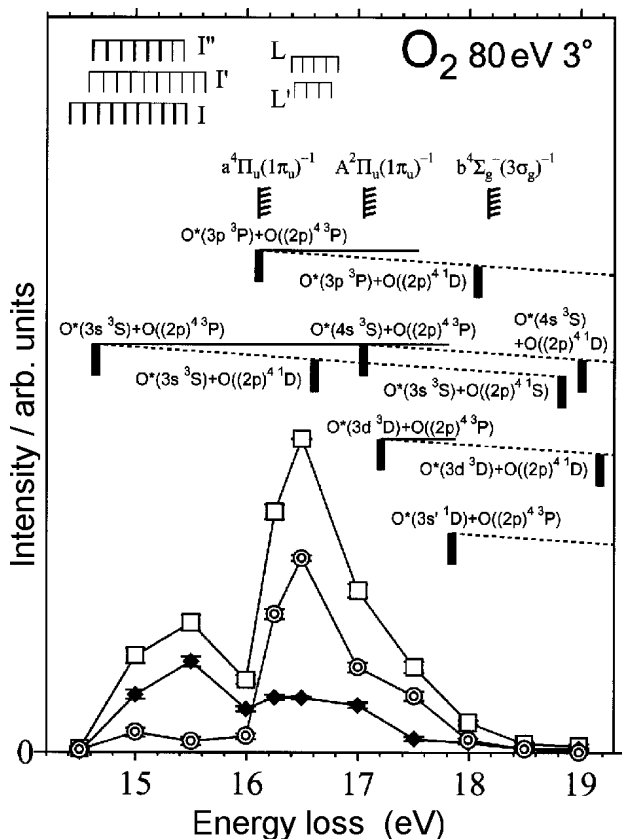


Fig. 8. The coincident electron-energy-loss spectrum of O_2 , i.e. the electron-energy-loss spectrum of O_2 tagged with VUV fluorescence, measured at 80 eV incident electron energy and 3° scattering angle. Open squares: the total spectrum, closed diamonds: the fast spectrum, and double circles: the slow spectrum, which are obtained from the summation over the total, fast, and slow ranges in Fig. 7, respectively (see the section of O_2). The resolution of the energy loss is approximately 250 meV. The dissociation limits to produce excited oxygen atoms emitting VUV fluorescence (see Table 2) are indicated by short vertical bars. The adiabatic ionization potentials of the $a^4\Pi_u(1\pi_u)^{-1}$, $A^2\Pi_u(1\pi_u)^{-1}$, and $b^4\Sigma_g^-(3\sigma_g)^{-1}$ states of O_2^+ are shown [11, 14] together with the energy levels of the I, I' and I'' series [12] and the L and L' series [10] observed in the photoabsorption spectra of O_2 .

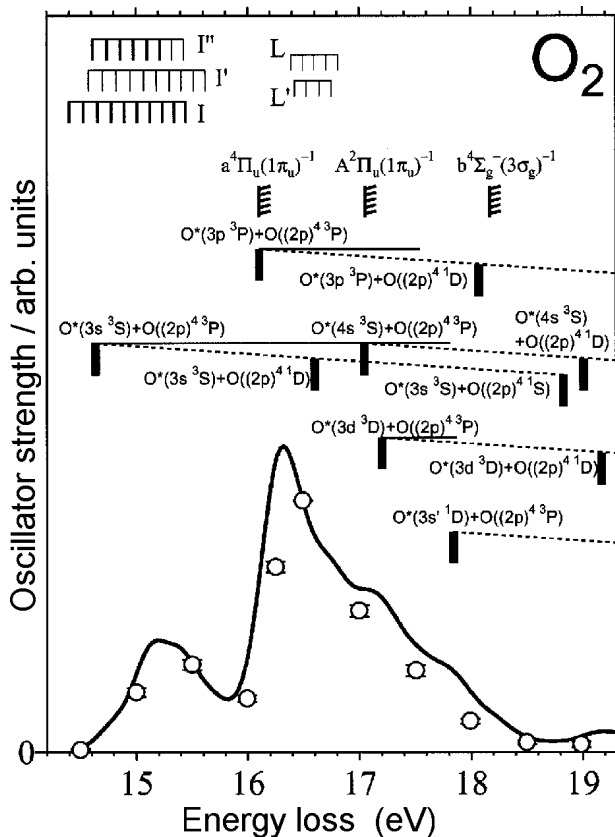


Fig. 9. The effective-GOS of O_2 for the emissive neutral-dissociation (open circles) obtained from the total coincident electron-energy-loss spectrum measured at 80 eV incident electron energy and 3° scattering angle in Fig. 8 and the DOS of O_2 for the emissive neutral-dissociation (solid curve) [15]. Two oscillator strengths are normalized at 16.49 eV energy loss. The resolution of the energy loss is approximately 250 meV. The dissociation limits, adiabatic ionization potentials, and energy levels involved are the same as in Fig. 8.

from the dispersed fluorescence spectra in the VUV range in the photoexcitation of O_2 , where the 130 nm line emitted by $O^*(3s^3S)$ plays an important role in the range of the incident photon energy 14.6–17.5 eV. The result of the comparison is shown in Fig. 9. The original DOS curve is folded with the energy-loss resolution of the present apparatus, approximately 250 meV, and the folded one is compared with the effective-GOS curve since the original one was measured with a much better resolution of the incident photon energy, 29 meV at 16.5 eV incident photon energy. The two oscillator strengths are normalized at 16.49 eV energy loss. It is clearly shown in Fig. 9 that the shape of the effective-GOS for the emissive neutral-dissociation at 80 eV/ 3° is in good agreement with the shape of the DOS for the same process, which indicates that the contribution of forbidden superexcited states is negligible in Fig. 8. Thus the peak around 15.5 eV energy loss in Fig. 8 seems to be attributed to the allowed superexcited states, probably those in the I, I' and I'' series [12, 30], and the peak around 16.5 eV energy loss seems to be attributed to the allowed superexcited states, probably those in the L and L' series [10].

In the investigation of the single-hole one-electron superexcited states of O_2 , we have been able to establish a new possibility of the coincident electron-energy-loss

spectroscopy, i.e. the time-resolved coincident electron-energy-loss spectrum as shown, for example, in Fig. 6, which give more knowledge on the decay processes of the superexcited molecules involved.

Conclusion

We have investigated both allowed and forbidden doubly-excited states of H_2 , D_2 and N_2 in much more detail than before by means of the coincident electron-energy-loss spectroscopy that we developed. It has been substantiated that the structures due to the doubly-excited states become highlighted in the energy-loss spectra tagged with the VUV fluorescence from neutral fragments, and thus the coincident electron-energy-loss spectroscopy is a key tool for investigating doubly-excited molecules. The comparison with the photoexcitation experiments of the same emissive neutral-dissociation by means of the oscillator strengths gives us clear discrimination between the allowed and forbidden doubly-excited states.

A new possibility of the coincident electron-energy-loss spectroscopy has been established in the investigation of the single-hole one-electron superexcited states of O_2 : the time-resolved coincident electron-energy-loss spectrum of O_2 has been measured at 80 eV incident electron energy and 3° scattering angle. The spectrum enables us to distinguish between the direct production process of $O^*(3s\ ^3S)$ and indirect one due to the cascade transition from $O^*(3p\ ^3P)$ to $O^*(3s\ ^3S)$.

We note that the coincident electron-energy-loss spectroscopy is powerful also in the investigation of highly excited states of molecules just below the first ionization potential (e.g. [18]).

Acknowledgments The support of the Ministry of Education, Culture, Sports, Science and Technology of Japan and Japan Society for the Promotion of Science in providing Grant-in-Aid for Specially Promoted Research, No. 08102005, and that for Scientific Research (B), No. 13440175, respectively, is greatly appreciated.

References

- Arai S, Yoshimi T, Morita M *et al.* (1986) Lyman- α excitation spectra in the photodissociation of the doubly excited states of H_2 . *Z Phys D: At Mol Clusters* 4:65–71
- Chan WF, Cooper G, Brion CE (1993) Absolute optical oscillator strengths for the photoabsorption of molecular oxygen (5–30 eV) at high resolution. *Chem Phys* 170:99–109
- Chan WF, Cooper G, Sodhi RNS, Brion CE (1993) Absolute optical oscillator strengths for discrete and continuum photoabsorption of molecular nitrogen (11–200 eV). *Chem Phys* 170:81–97
- Glass-Maujean M (1986) Photodissociation of doubly excited states of H_2 , HD, and D_2 . *J Chem Phys* 85:4830–4834
- Glass-Maujean M (1988) Photodissociation of doubly excited states of H_2 : Emission of Balmer lines. *J Chem Phys* 89:2839–2843
- Guberman SL (1983) The doubly excited autoionizing states of H_2 . *J Chem Phys* 78:1404–1413
- Hatano Y (1999) Interaction of vacuum ultraviolet photons with molecules. Formation and dissociation dynamics of molecular superexcited states. *Phys Rep* 313:109–169
- Hatano Y (2001) Interaction of VUV photons with molecules: Spectroscopy and dynamics of molecular superexcited states. *J Electron Spectrosc Relat Phenom* 119:107–125
- Huber KP, Herzberg G (1979) Molecular spectra and molecular structure IV. Constants of diatomic molecules. Van Nostrand Reinhold, New York
- Huffman RE, Larrabee JC, Tanaka Y (1964) Absorption coefficients of oxygen in the 1060–580 Å wavelength region. *J Chem Phys* 40:356–370
- Itikawa Y, Ichimura A, Onda K *et al.* (1989) Cross sections for collisions of electron and photons with oxygen molecules. *J Phys Chem Ref Data* 18:23–42
- Katayama DH, Tanaka Y (1981) The I, I', and I'' absorption bands of O_2 in the region 790–865 Å. *J Mol Spectrosc* 88:41–50
- Kouchi N, Ukai M, Hatano Y (1997) Dissociation dynamics of superexcited molecular hydrogen. *J Phys B: At Mol Opt Phys* 30:2319–2344
- Krupenie PH (1972) The spectrum of molecular oxygen. *J Phys Chem Ref Data* 1:423–534
- Machida S (1997) Dynamics of dissociation and ionization of molecules via superexcited states. PhD Thesis, Tokyo Institute of Technology
- Martin F (1999) Non-autoionizing doubly excited states of H_2 : the Σ^- symmetry. *J Phys B: At Mol Opt Phys* 32:L181–L187
- Nakamura H (1991) What are the basic mechanisms of electronic transitions in molecular dynamic processes? *Int Rev Phys Chem* 10:123–188
- Odagiri T, Koyama K, Uemura N, Kouchi N, Hatano Y (1999) Predissociation of optically forbidden states in electron-hydrogen collisions as studied by coincident electron energy-loss spectroscopy. *J Phys B: At Mol Opt Phys* 32:1335–1344
- Odagiri T, Takahashi K, Yoshikawa K, Kouchi N, Hatano Y (2001) Forbidden doubly excited states of molecular nitrogen dissociating into two neutral atoms in electron collisions. *J Phys B: At Mol Opt Phys* 34:4889–4900
- Odagiri T, Uemura N, Koyama K, Ukai M, Kouchi N, Hatano Y (1995) Electron energy-loss study of superexcited hydrogen molecules with the coincidence detection of the neutral dissociation. *J Phys B: At Mol Opt Phys* 28:L465–L470
- Odagiri T, Uemura N, Koyama K, Ukai M, Kouchi N, Hatano Y (1996) Doubly excited states of molecular hydrogen as studied by coincident electron-energy-loss spectroscopy. *J Phys B: At Mol Opt Phys* 29:1829–1839
- Radzig AA, Smirnov BM (1985) Reference data on atoms, molecules and ions. Springer Verlag, Berlin
- Sharp TE (1971) Potential-energy curves for molecular hydrogen and its ions. *Atomic Data* 2:119–169
- Shimamura I, Noble CJ, Burke PG (1990) Complex quantum defects of superexcited Rydberg states of H_2 . *Phys Rev A* 41:3545–3554
- Striganov AR, Sventitskii NS (1968) Tables of spectral lines of neutral and ionized atoms. Plenum, New York
- Tennyson J (1996) Resonance parameters and quantum defects for superexcited H_2 . *Atom Data Nucl Data Tables* 64:253–277
- Uemura N, Odagiri T, Hirano Y, Makino Y, Kouchi N, Hatano Y (1998) Isotope effects in the dynamics of doubly excited states of molecular hydrogen and deuterium as studied by coincident electron-energy-loss spectroscopy. *J Phys B: At Mol Opt Phys* 31:5183–5196
- Ukai M, Kameta K, Kouchi N, Hatano Y, Tanaka K (1992) Neutral decay of double-holed doubly excited resonances of N_2 . *Phys Rev A* 46:7019–7022
- Wiese WL, Fuhr JR, Deters TM (1996) Atomic transition probabilities of carbon, nitrogen, and oxygen. A critical data compilation. *J Phys Chem Ref Data, Monograph* 7:1–522
- Wu CYR (1987) Assignments of autoionization states of O_2 . *J Quant Spectrosc Radiat Transfer* 37:1–15